

**COMPARISON OF TWO DIFFERENT RAY TRACING ALGORITHMS
FOR TOMOSYNTHESIS**

**M.Sc. Thesis by
Emine CAN**

Department : Electronics and Communication Engineering

Programme : Biomedical Engineering

Thesis Supervisor: Asst. Prof. Dr. Mustafa KAMAŞAK

MAY 2011

**COMPARISON OF TWO DIFFERENT RAY TRACING ALGORITHMS
FOR TOMOSYNTHESIS**

**M.Sc. Thesis by
Emine CAN
(504091412)**

**Date of submission : 06 May 2011
Date of defence examination: 26 July 2011**

**Supervisor (Chairman) : Asst. Prof. Dr. Mustafa Ersel KAMAŞAK
(ITU)
Members of the Examining Committee : Assoc. Prof. Dr. Uluğ BAYAZIT (ITU)
Asst. Prof. Dr. İlker BAYRAM (ITU)**

MAY 2011

İSTANBUL TEKNİK ÜNİVERSİTESİ ★ FEN BİLİMLERİ ENSTİTÜSÜ

**TOMOSENTEZ İÇİN İKİ FARKLI IŞIN İZLEME YÖNTEMİNİN
KARŞILAŞTIRILMASI**

**YÜKSEK LİSANS TEZİ
Emine CAN
(504091412)**

**Tezin Enstitüye Verildiği Tarih : 06 Mayıs 2011
Tezin Savunulduğu Tarih : 26 Temmuz 2011**

**Tez Danışmanı : Yrd. Doç. Dr. Mustafa Ersel
KAMAŞAK(İTÜ)
Diğer Jüri Üyeleri : Doç. Dr. Uluğ BAYAZIT (İTÜ)
Yrd. Doç. Dr. İlker BAYRAM (İTÜ)**

Mayıs 2011

FOREWORD

First of all, I would like to thank my supervisor Asst. Prof. Dr. Mustafa E. Kamaşak for the opportunity he gave me to write my thesis on this topic and for sharing his expert knowledge in programming on image processing.

Secondly, thanks to the EU LLP Erasmus Exchange Programm, I got the chance to collaborate with the Department of Biomedical Engineering at Linköping University, Sweden. I am very grateful to Prof. Hans Knutsson who made invaluable contributions on improving my results and I thank Mats Andersson for his ideas and guidance.

I owe thanks to my classmates from master programme at Istanbul Technical University for keeping up the good spirit for two years and for their help and support during my exchange period. I have special thanks to Yasemin Koray who helped me to form fancy sentences in seconds.

Since I am a member of EESTEC (Electrical Engineering Students' European Association) I have been "so sophisticated" and motivated in whatever the challenge is in my life. Thank you my boardies and all my friends who have the EESTEC spirit inside.

And lastly, many thanks goes to my extended family for their neverending support and encouragement not only during this study but also all through my life.

May 2011

Emine Can

Electrical & Electronics Engineer

TABLE OF CONTENTS

	<u>Page</u>
TABLE OF CONTENTS	vii
ABBREVIATIONS	ix
LIST OF TABLES	xi
LIST OF FIGURES	xiii
SUMMARY	xv
ÖZET	xvii
1. INTRODUCTION	1
1.1 Breast Cancer	1
1.2 Breast Cancer Diagnosis: History and Evolution.....	3
1.3 Physical Factors that Affect Image Quality in Mammogram.....	5
1.4 Digital Mammography	7
1.4.1 Advance Applications	10
1.5 Tomosynthesis.....	11
1.5.1 Reconstruction Algorithms Used in Tomosynthesis.....	14
1.5.1.1 Algebraic Reconstruction Techniques	15
1.5 Hypothesis	19
2. BACKGROUND	20
2.1 Ray Tracing	20
2.1.1. Siddon's Algorithm.....	20
2.1.2. Gaussian Algorithm	25
3. METHODOLOGY	28
3.1 Results	33
4. CONCLUSION	41
REFERENCES	43
CURRICULUM VITAE	47

ABBREVIATIONS

SFM	: Screen-film mammography
DM	: Digital mammography
CAD	: Computer aided detection/diagnosis
CCD	: Charge-coupled device
TFT	: Thin-film transistor
CT	: Computed tomography
2D	: Two-dimensional
3D	: Three-dimensional
DQE	: Detective quantum efficiency
SAA	: Shift and add
MITS	: Matrix inversion tomosynthesis
FB	: Filtered backprojection
SART	: Simultaneous algebraic reconstruction technique
ART	: Algebraic reconstruction techniques
SIRT	: Simultaneous iterative reconstruction technique
CS	: Compressive sensing
TV	: Total variation
GP	: Gaussian parameter
RMSE	: Root Mean Square

LIST OF TABLES

Page

Table 3.1: RMSE Comparison of the two ray tracing algorithms for full angle of view.....36

Table 3.2: Comparison of RMSE values for Siddon and Gaussian algorithms.....39

LIST OF FIGURES

	<u>Page</u>
Figure 1.1: Incidence of the Most Common 10 Types of Cancer in Women, (per 100.000, World Standard Population), Turkey, 2006-2008	2
Figure 1.2: Illustration of contrast derivation (a) in case of no scatter or noise (b) in presence of scattered radiation.....	6
Figure 1.3: Basic components of a digital mammography system.	8
Figure 1.4: Tomographic geometry	13
Figure 1.5: Principle of shift and add tomosynthesis	13
Figure 1.6: The square grid used in algebraic methods.....	16
Figure 2.1: Geometric illustration of a ray on image grid	21
Figure 2.2: Smoothing with Gaussian form.....	27
Figure 2.3: Geometric representation of the Gaussian algorithm.....	27
Figure 3.1: Squeezing process.....	29
Figure 3.2: Flow chart of the SART algorithm.....	30
Figure 3.3: Frame application.....	32
Figure 3.4: Flow chart of the SART algorithm with frame application.....	33
Figure 3.5: Convergence of the two ray tracing algorithm	34
Figure 3.6: Comparison of the two ray tracing algorithms for full angle of view.....	35
Figure 3.7: Results of the Siddon Algorithm.....	37
Figure 3.8: Results of the Gaussian Algorithm.....	38
Figure 3.9: Frame application results for Gaussian algorithm.....	36

COMPARISON OF TWO DIFFERENT RAY TRACING ALGORITHMS FOR TOMOSYNTHESIS

SUMMARY

Breast cancer is a major health problem worldwide which comes in the first rank as a cause of death in women. In breast cancer diagnosis, the transition of mammography from screen-film to digital form has made many advantages available. Especially with the introduction of new digital flat panel detectors, new algorithms which improves image quality became available. The objective of this study is to form a new ray tracing algorithm for image reconstruction and compare the reconstructed image quality with the results of known ray tracing model of Siddon. Tomographic reconstruction is modelled with simultaneous algebraic reconstruction technique which is a way of reconstruction in tomosynthesis. The experiments are applied to two dimensional images and also the algorithm is designed in the form that it can be easily modified to three dimensional detection. The whole project is firstly inspired by limited view of angle which is one of the main problems in breast tomosynthesis. Thus the experiments also consider the results of limited angle of view projection case. All of the algorithms and experiments are programmed and simulated with Matlab. Although efficacious results are obtained with both of the algorithms, a drawback with the newly developed model is the lack of contrast in low frequencies. In addition it is realized that even the ray tracing algorithms are fast, the iterative property of algebraic reconstruction technique makes the process ever time consuming which does not let to work with images in larger size.

TOMOSENTEZ İÇİN İKİ FARKLI IŞIN İZLEME ALGORİTMASININ KARŞILAŞTIRILMASI

ÖZET

Meme kanseri dünya çapında önemli bir sağlık sorunudur. Kadınlarda ölüm nedenleri arasında ilk sırada yer alır. Mamografinin film teknolojisinden sayısal hale geçişi meme kanseri teşhisine bir çok avantaj sağlamıştır. Özellikle yeni sayısal panel algılayıcıların ortaya çıkması ile görüntü kalitesini artıracak gibi yeni algoritmaların uygulanabilmesi mümkün hale gelmiştir. Bu çalışmanın amacı görüntü elde etmede yeni bir ışın izleme algoritması oluşturmak ve sonuçlarını Siddon'un bilinen ışın izleme modeli ile karşılaştırmaktır. Deneyler iki boyutlu görüntüler için uygulanmıştır ve oluşturulan algoritmalar üç boyutlu görüntülere de kolaylıkla uyarlanabilecek şekilde tasarlanmıştır. Tüm bu proje ilk olarak meme tomosentezinde temel problemlerden biri olan sınırlı açı projeksiyonundan ilham almıştır. Bu nedenle deneyler sınırlı açı projeksiyon koşulunun sonuçlarını da kapsar. Tüm algoritmalar ve deneyler Matlab ile programlanmış ve gerçekleştirilmiştir. Etkili sonuçlar elde edilmesine rağmen yeni geliştirilen algoritmanın yüksek frekanslarda görüntünün kontrastını azalttığı gözlemlenmiştir. Aynı zamanda, ışın izleme algoritmaları hızlı işlem yapacak şekilde tasarlanmış olmasına rağmen kullanılan cebirsel görüntü elde etme algoritmasının tekrarlı yapısının işlemin toplam süresini büyük boyutlu görüntüler ile kolay çalışamayacak şekilde uzattığı gözlemlenmiştir.

1. INTRODUCTION

1.1 Breast Cancer

Breast cancer named as carcinoma is the most encountered type of cancer among women in Turkey, ranking the first place (41.6), followed by colorectal (15.3), thyroid (13.5) and uterine-cornus (8.7) cancer (per 100 thousand) in 2008 as shown in Table 1.1. According to the data retrieved from Ministry of Health Department of Cancer Control, although breast cancer does not take place in the top ten cancer types of men, it is stated in the fourth rank with 17,96 per 100 thousand in the frequent cancer types in Turkey. Also it ranks the 8th with a ratio of 2.1 % within 20 diseases which most frequently result in death in females. The rate of age-standardized case studies show that women older than the age of 45 has a higher risk of breast cancer, constituting 87% of all the age groups [1, 2]. In Yılmaz *et al* it is reported that in 2005, 22% of the population of Turkey was above 45 and it is estimated that this ratio will rise to 32% in 2030 [3]. Hence, breast cancer will maintain its importance in coming years. World Health Organization provides the statistics of deaths by age, gender and cause for the year 2004 shows breast cancer is the first cause of death in cancer types for women above 30 in the world. The remarkable point is, while the ratio of deaths caused by breast cancer is 31% in high income countries, it is 69% in the rest as estimated in 2004. On the contrary, incidence of breast cancer is not very different (44% in high income, 56% lower income) [4]. Therefore, it is obvious that the early detection of breast cancer with mammography screening supported by the government to get the treatment affordable and easy to access decreases mortality. This is the reason for the women in western Europe, America and Australia, to survive with the breast cancer by the health regulations on this issue starting from 1970s. With the positive effects of the latest regularities on free breast cancer screening in Turkey in 2005, number of mammography examinations performed is increased 59% in between 2007 and 2009 [2].

The early detections by these regulations have made the incidence statistics more clear and reduced the cost of treatment. Moreover and most important result is an increase in the life quality of women.

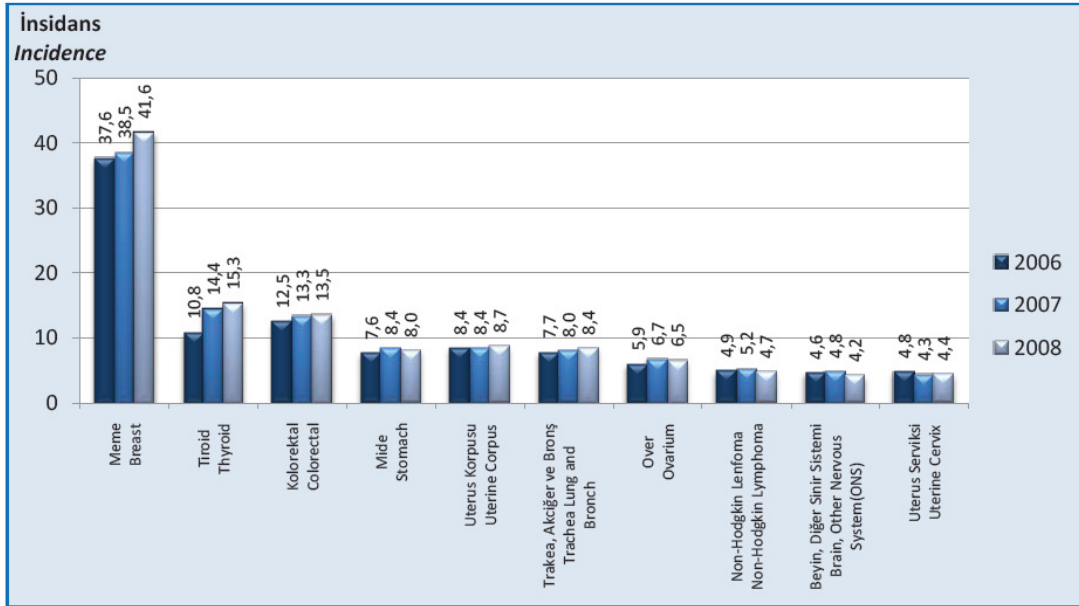


Figure 1.1: Incidence of the Most Common 10 Types of Cancer in Women, (per 100.000, World Standard Population), Turkey, 2006-2008.

1.2 Breast Cancer Diagnosis: History and Evolution

Mammography is one of the most common, reliable and demanding radiological techniques in non palpable breast cancer detection. However the breast is one of the most radiosensitive parts of the body. Therefore, the detection must be done at the lowest radiation dose with the optimal image quality. There are several physical factors affecting the image quality of mammogram such as scattered radiation, motion artefacts and compression of the breast. Besides, breast tumors at younger ages may not be distinguishable because of the dense structure of the breast tissue caused by active milk glands. Image processing algorithms and detector electronics are the main research areas to overcome these factors and to obtain better image quality [5].

History of mammography dates back to 1913 when Albert Salomon, a surgeon, reported his studies on using radiography on mastectomy specimens to demonstrate the spread of the tumor on axillary lymph nodes. He also showed that highly infiltrating carcinoma could be radiographically distinguished from circumscribed carcinoma. After decades, in 1930, Stafford L. Warren, a radiologist's report on the use of stereoscopic technique for in vivo mammography using a device with higher technology which had a moving grid to diminish scattered radiation.

During 1930s, several studies about imaging and differentiating the benign breast lesions from carcinoma were reported. These studies suggest that a considerable improvement of the roentgen method would be necessary before it can be regarded as a superseding diagnostic aid in early stages of breast pathology. Until 1940s surgeons were active on trials of breast imaging with x-ray which started the first ideas of mammography and this stage is considered as the first period in the history of developing mammography.

Oncoming 1950s the physical factors that affect the image contrast came in sight and in 1953 Paul Leborgne recognized the importance of breast compression on image quality. Different methods were tried to obtain adequate exposure of thinner and thicker tissues in breast. Although roentgen has been known since 1895, there was no specific knowledge of the mammography technique which was described as simple soft tissue roentgenography of the breast until 1960s.

In 1960 Robert L. Egan described a high milli-ampere, low kilo-voltage mammographic technique that used industrial film which was easily reproducible.

In May 1963, mammography is accepted as a useful and reproducible technique developed by Egan, which could enable differentiation between benign and malignant lesions and could be used to screen for cancer in asymptomatic women at a conference supported by Cancer Control Program of the U.S. Public Health Service. The years between 1940 and 1970 is known as second stage as the radiologists were joined to the process of mammography developing after surgeons.

In the third stage which ends with the last quarter of the 20th century was the stage of fast improvements especially on detector and film side. Besides radiologists, the private companies were joined to the development and it was DuPont who became the first company to market a dedicated screen-film mammography system and a device for creating a vacuum to hold the screen and film together. Eastman Kodak followed with its own screen-film mammography unit and introduced a vacuum cassette mammography in 1970's. In Sweden and USA, mammography devices began to be used for public health with mammography screening vans and it showed that early detection decreased the mortality rate [6, 7].

Screen-film mammography (SFM), which uses a fluorescent screen that absorbs X-Rays and converts them to light that is recorded on photographic film, is to be a reference for breast imaging quality today. However, the increased development in digital X-Ray radiography superseded SFM with digital mammography (DM) which avoids limited sensitivity in breast cancer detection. Actually, X-ray examination of the breast has been the last area of roentgenology at the transition between analog to digital imaging [8].

The computerization of image acquisition, display and storage, thus enabling better communication capabilities are the first advantages of the DM. Within the last 10 years, comparative studies [9-12] investigated that, DM performs as well as or better than SFM and accepted it as a valid alternative. Compared to standard SFM, DM has a higher cancer detection rate, a significantly lower recall rate, a significantly higher positive predictive value, and uses lower average glandular dose. In Gennaro's study it is stated that average glandular dose is reduced 27% of digital over SFM [13]. The dose savings are about 15% for thin and thick breasts and it is between 30% and 40% for intermediate thickness. This reduction is admitted by higher efficiency of

digital detector which can be exposed at higher energy spectra than SFM and by the separation between acquisition and displaying process. In the Digital Mammographic Imaging Screening Trial conducted by the American College of Radiology Imaging Network has confirmed previous results that digital mammography was significantly better than conventional film mammography at detecting breast cancer in young women, premenopausal and perimenopausal women, and women with dense breasts. There was no significant difference in diagnostic accuracy between digital and film mammography in the population as a whole or in other predefined subgroups. However, digital mammography offers other advantages over film mammography, namely, easier access to images and computer-assisted diagnosis; improved means of transmission, retrieval, and storage of images; and the use of a lower average dose of radiation without a compromise in diagnostic accuracy [14].

SFM has limitations on its efficiency by its dynamic range, low contrast resolution, film noise, dose-inefficient scatter reduction, and film processing artifacts [15]. DM enables the separation of image acquisition, processing and display and most advantageous part is it allows optimization of each of these steps. In addition, advanced applications such as computer aided detection/diagnosis (CAD) can be easily implemented to the digital mammography [16].

1.3 Physical Factors That Affects Image Quality in Mammography

Mammographic image is required to have excellent spatial resolution and contrast sensitivity to make microcalcifications and subtle lesions visible. The limitation is the radiosensitivity of the breast which is very high and this shackles more dose application. There are some physical factors that effect the quality of image in mammography. The most important factors are scattered radiation, noise, and compression of breast. Image processing algorithms are also important in terms of image quality and radiation dose.

The effect of scattered radiation can be explained with the change in contrast. Contrast is defined as the change in the initial x-ray attenuation due to a difference structure inside the tissue which is explained by Figure 1.1.

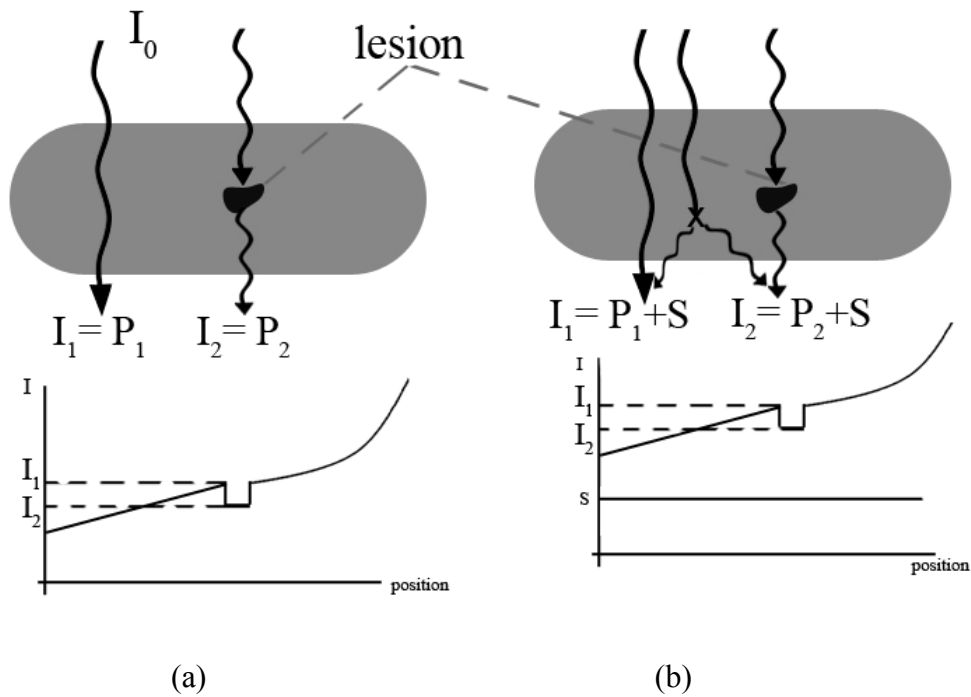


Figure 1.2: Illustration of contrast derivation (a) in case of no scatter or noise (b) in presence of scattered radiation.

In Figure 1.1 (a) the effects of scattered radiation is ignored so the detected radiation signal is directly the initial one or the attenuated one itself. In this case the contrast is calculated as follows;

$$contrast = \frac{I_2 - I_1}{I_1 + I_2} = \frac{P_2 - P_1}{P_1 + P_2} \quad (1)$$

where I_0 is the initial radiation, I is the total radiation, P is the primary radiation signal and S is the uniform scatter intensity.

In Figure 1.1 (b) shows how to determine the contrast in presence of scattered radiation. The contrast decreases as it is obvious with the following formula;

$$contrast = \frac{(P_1 + S) - (P_2 + S)}{(P_1 + S) + (P_2 + S)} = \frac{P_2 - P_1}{P_1 + P_2 + 2S} \quad (2)$$

The scattered radiation cancels in the numerator but adds in the denominator which reduces the contrast of the image. This effect is larger when the object is thicker so that the compression became a compulsory process during breast imaging.

Noise is also an important factor that effects the image quality and may cause the fluctuation of the detected x-rays and makes image less reliable. A solution to this problem is to increase the number of detected x-rays. It is possible with improved detectors which are the receptors with high quantum efficiency with the detectors who have slow receptors which needs more quanta to form the image.

Compression of the breast is another factor influencing image quality. Compression makes the atomic structures spread out and breast becomes thinner and more uniform in attenuation. Thus superposition of shadows decreases and perceptability of sturctures increases. Despite these benefits, compression is unfavorable because it is at first uncomfortable for the patient and also it causes misalignments in 3D acqusition [17].

1.4 Digital Mammography

Physics of digital mammography (DM) shows no difference from SFM but the detector part. In Figure 1.2, basic components of mammography system are illustrated schematically. A divergent beam of X-ray photons are generated from the source which has a focal spot and anode that are situated above the chest wall of the patient. The small focal spot size and the large distance from X-ray source to breast, mean that it is reasonable to model the source as an infinitesimal spot. and the beam is directed to the compressed breast. This beam is filtered with aliminium or equivalent filters to remove low energy photons, thus reduces unnecessary exposures to the patient. The beam is focused to the area of interest with the collimator. Breast compression is the major source causes patient discomfort but brings advantages on image like more uniform breast thickness resulting in better film latitude or dynamic range, prevents motion artifacts, reduces scattered radiation that improves contrast sensitivity, better visualization of the tissue near the chest wall

and reduces radiation dose. A gridding operation is usually applied to the X-ray photons leaving the breast before they reach the digital detector to eliminate scattered photons [18-20] .

Various types of detector mechanisms that are being used in today's DM systems can be grouped in five different types: flat-panel phosphor system, scanning phosphor charge-coupled device (CCD) system, computed radiography system, selenium flat-panel system and newly developed photon counting detectors.

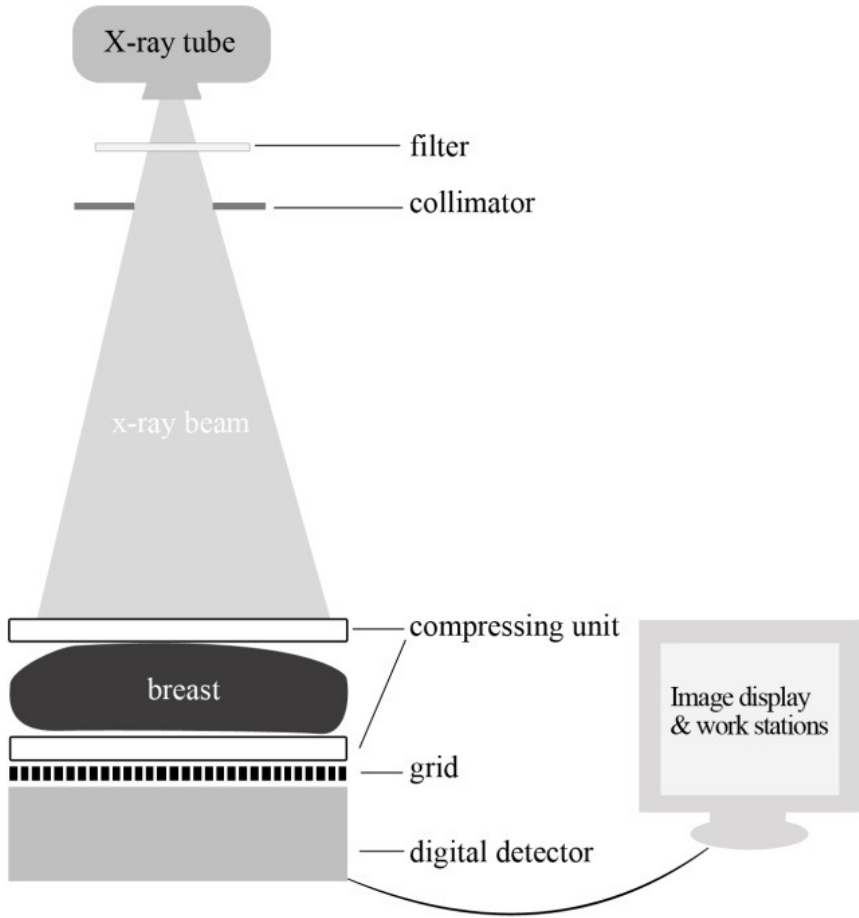


Figure 1.3: Basic components of a digital mammography system.

In flat-panel phosphor detector system, x-rays are absorbed by a CsI(Tl) phosphor layer. An array of photodiodes which is formed on an amorphous silicon plate are used to record the light emitted by the phosphor. Each photodiode is connected to

thin-film transistor (TFT) that is connected to a series of control lines. Senographe 2000D (GE Medical Systems) is an example for this class. This type of detector can perform rapid-sequence imaging but has the disadvantages on the cost and the difficulty in further reducing detector element.

In scanning phosphor CCD system, (SenoScan system -Fischer Medical Imaging), x-ray beam is detected by a slot shaped detector which uses CsI(Tl) phosphor. The phosphor is coupled through a fiberoptic plate to a CCD where the light is converted into electrical signal. The fiberoptics protects the CCD from radiation damage. With the slot shaped detector scatter rejection with high efficiency is possible so grid is not required. In addition to its advantages, dose reduction is possible and due to the fewer elements it is less expensive. However, it requires a longer total image acquisition time-approximately 6 seconds- than that needed by the area detector and the x-ray tube heat loading is greater.

Computed radiography system manufactured by Fuji, employs a photo-stimulable phosphor plate, which is very similar in operation to the detectors that have been used for computed radiography. With the absorption of X-rays, electronic charges are stored in in the crystalline material of the phosphor. After exposure, the phosphor plate is removed and is read out by scanning with a fine helium–neon laser beam.

The red light from the laser causes emission of the blue light and it is collected with a photo-multiplier tube then digitized. Main advantages of the system are small detector size and ease of having multiple plate size. The scattering of laser light during read-out causes loss of spatial resolution and addition of noise during the low collection efficiency of emitted light are the disadvantages.

Selenium flat-panel system, manufactured by Hologic, has the difference in absorbing x-ray with amorphous selenium instead of phosphor. When x-ray photons are absorbed electron-hole pairs are formed and electric charge is released from this matter. Simple electrode pads collect the charge. The advantages of this system are the high modulation transfer function and detective quantum efficiency that can be achieved. The need for a high biasing voltage and the high cost of the detector are the main problems.

Photon counting technology is introduced in 2003 by Sectra Mamea with MicroDose Mammography system. In this system, x-ray beam is collimated to equidistant line beams that removes scatter radiation efficiently. Photon counting Si-strip detectors are designed to match the line beams. The strips are like a separate reversed bias PIN-diodes, depleted by a bias voltage, and no current flows unless photons interact in the sensor and create electron-hole pairs. Electrons and holes drift to the opposite sides of the detector. This drifting motion induces current and the counters which is bonded to strips are incremented if the pulse is above a threshold level. The main advantage of this counting system is the possibility to set the electronic threshold to eliminate the noise from the electronics [18-22].

1.4.1 Advanced applications

Besides the development of new detector technologies, there are ongoing developments on novel applications like tomosynthesis, contrast enhanced mammography, telemammography and CAD which are not possible with SFM.

Contrast enhanced mammography is a technique that identifies breast lesions by identifying abnormal blood vessel formations (angiogenesis) around carcinoma. DM is performed after iodinated contrast agent is injected intervenously. A subtraction procedure is applied to the image to get enhanced structures from the surrounding tissue [16].

The technology of CAD uses computer software to help the radiologist in the interpretation of mammographic abnormalities. CAD is commercially used both in SFM and DM. The digitization of the image is not required in DM before the application of CAD procedure, makes it faster than SFM.

Telemammography is the transmission of highquality mammographic images in digital form to different geographical locations over a telecommunication system with variety of methods like high-speed internet, satellite, or wireless links. Telemammography enables consultations among clinicians and is a chance for patients in underserved areas to have their mammograms interpreted by experts.

Tomosynthesis, which will be deeply demonstrated in the next section, is a technique for producing slice images using methods originated from conventional tomography. Tomosynthesis is particularly important as it improves the detection and characterization of lesions in overlying dense tissue in breasts [14, 16, 20].

1.5 Tomosynthesis

After the advent of computed tomography (CT) in 1970s, some of the limitations of two-dimensional (2D) radiography are overcome. The ability to depth localization, improved conspicuity and improved contrast of the structures of interest were the main facilities of this three-dimensional (3D) imaging technique. The operating principle of the tomographic imaging is, as illustrated in Figure 1.3, to obtain the image plane of interest by moving x-ray tube above the patient and the detector on opposite side, beneath the patient. The image plane is focused by being located at fulcrum of this motion. All other planes other than the plane of interest are acquired blurry. This blur from other planes obscures detail in the plane of interest and limits the contrast enhancement of the slices. Tomography was accepted to be advantageous for diagnostic imaging allowing a 3D orientation of anatomy to be understood and to bring the image plane of interest out from the structures in other planes which obstruct clear detection. However, the acquisition of only one slice at one exposure time generated the problem of the excessive patient dose and time requirement to image entire volume of data. In addition, the blurring problem required complex mechanical motions to adjust the fulcrum like linear, circular and even hypocycloidal motion. Another limitation, collecting image projections over 360° is not always possible, on account of organ location with C-arm systems, which are restricted to 205° rotation. Limited view methods, such as digital tomosynthesis are introduced to overcome these limitations of 3D imaging of conventional tomography [22-24].

Tomosynthesis is referred to as limited angle CT, a 3D imaging technique which allows retrospective reconstruction of an arbitrary number of tomographic planes in a limited angle of view with reduced cost and dose [24, 25]. The system architecture is not very different from CT but only the reconstruction methods. X-ray tube moves across an arc and enables multiple 2D projections within a limited angle at varying orientations of x-ray tube, patient and detector. Generally it is performed using 10 to 25 projections over an angle of 15° to 50° . The volumetric image is reconstructed from the 2D projections using algorithms like “shift and add”. Enhancement of the information contained in each plane of interest is provided by varying the amount of

shifting. The reconstruction algorithms of tomosynthesis combines the images enabling the image information to be additive, that makes tomosynthesis a low-dose imaging technique [24-26]. Tomosynthesis was first introduced by Grant in 1972 based on the work of conventional tomography [27]. Despite the known advantages mentioned above, it became possible to implement the system practically after the advent of flat-panel detectors which have large-area, high frame rate and exceptional detective quantum efficiency (DQE) and provide low electronic noise and fast-read out times thus enabling rapid acquisition of a large number of low-dose projection images, in the last decade. Research and clinical interest on digital tomosynthesis is renewed with the development of various digital detectors [24-25].

Tomosynthesis is accepted as a way to decrease mammographic false negatives caused by overlapping normal breast tissue obscuring cancers. It allows to improve the detection of subtle lesions, and permits the characterization of masses and of density asymmetry and the accurate measurement of breast lesion by a better delineation of the lesion borders. In addition, false positives resulting from overlapping tissue appear similar to breast lesions may also be reduced. Therefore tomosynthesis has the potential to increase sensitivity and specificity with improved visibility and improve early breast cancer detection in women with dense breasts [22,26,28].

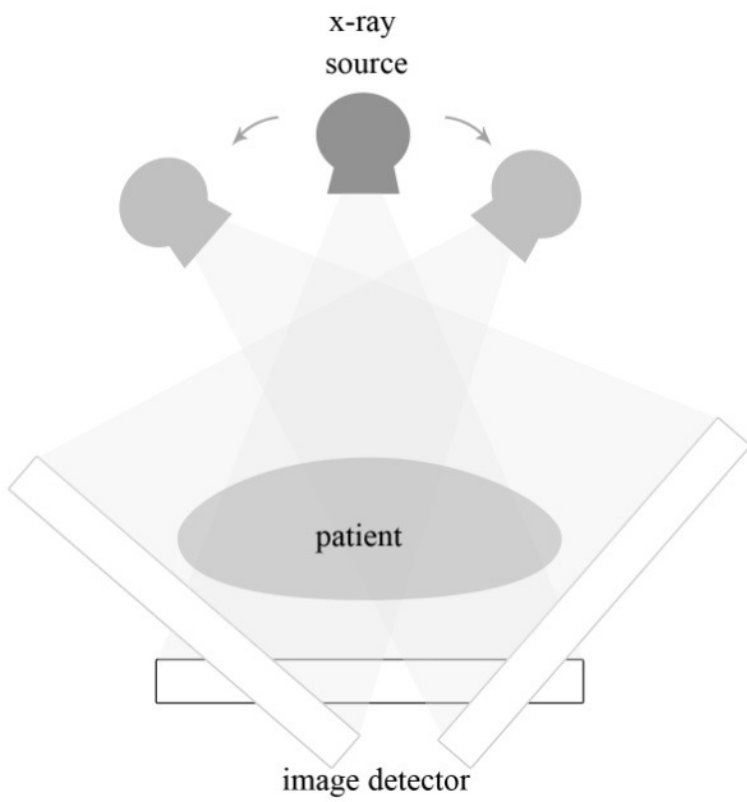


Figure 1.4: Tomographic geometry

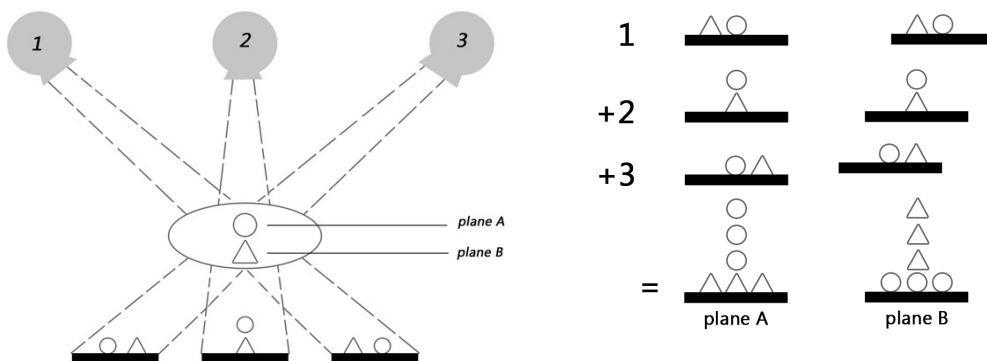


Figure 1.5: Principle of shift and add tomosynthesis

1.5.1 Reconstruction Algorithms used in Tomosynthesis

Several reconstruction algorithms are being used in tomosynthesis to overcome the problems resulted from limited angle of view or deblurring from overlying tissues. The main parts of all the algorithms described below depends on geometric behaviour of the x-ray system. The earliest and mostly common reconstruction method in tomosynthesis is known as shift and add (SAA). It is obvious that in a system which the x-ray source and the detector moves synchronously in a parallel plane, on detected images, the magnification of the objects at different locations at z-direction will depend only on their height above the detector. SAA is an algorithm uses this fact to bring sharp focus in plane of interest, which generates a set of slice images by summation of the projections acquired by different positions of x-ray source and detector with predefined amount of shifting as illustrated in Figure 1.4. The shifting must be correctly performed to avoid missalignment. Although the mechanical systems allows right shifting, the artifacts originated from patient motion effects the alignment. In breast tomosynthesis it is avoided by breast compression supports. In image reconstruction of tomosynthesis two main challenging problems are at issue: superimposition induced blurry images and lack of samples resulted from limited view of angles. SAA is a simple algorithm but not sufficient to perform full contrast images. The focal plane includes blurred out objects from other planes with superimposition.

In this context two deblurring reconstruction algorithms are presented that are matrix inversion tomosynthesis (MITS) and filtered backprojection (FB). Apart from the summation and fourier techniques, algebraic methods have particularly important role in limited view of angle tomography. The drawback of FB requires sufficient projection data with low noise level to recover the 3D images. In this manner, iterative reconstruction techniques, like simultaneous algebraic reconstruction technique (SART), are superior to FB with noise removal and less data requirement. Nonlinear regularization methods are also implementable to these techniques as comparable to the filters in FB [20].

Unblurred objects are obtained solving matrix algebra by predefining a blurring function for all planes except the tomosynthesized one. It performs well in imaging mid and high spatial frequency components of the image. FB is simply performed as smearing back the detected line integral of attenuation coefficients at each pixel. It is repeated for every projection angle resulting a simple backprojection of the image. Due to the limited number of samples of the projected data, a ramp filter is needed to be applied to the resulted image. FB has better noise reduction at low frequencies than MITS [24].

Another approach based on reconstruction in fourier domain is ectomography, a method of acquiring slices by summing 2D projections of the object filtered orthogonally by low pass and high pass filters. In a circular tomographic geometry, each projection image is high pass filtered and summed. The signal strength of the structures projected along a circular path are weakened enabling deblurring. A low pass filter is also applied in orthogonal dimensions with the high pass filter to each projection image to get more uniform impulse response in the z direction and to make the image plane of interest appear unfiltered [24].

1.5.1.1 Algebraic Reconstruction Techniques

Algebraic reconstruction techniques (ART) are accepted as an alternative solution to the limited angle reconstruction problem where it is not possible to acquire sufficient number of or uniformly distributed projections to form the whole 3D image. The formulation of ART is based on a grid geometry with N cells as illustrated in Figure 1.4. The term *ray-sum* takes the place of the line integral in transform-based methods. The ray-sum, p_i , measured with the *ith* ray, is expressed as;

$$\sum_{j=1}^N w_{ij} f_j = p_i \quad \begin{matrix} i = 1, 2, \dots, M \\ j = 1, 2, \dots, N \end{matrix} \quad (3)$$

where w_{ij} is the weighting parameter which stands for the influence of j th cell on the i th ray line integral, f_j is the constant intensity value of the j th cell and M is the total number of rays.

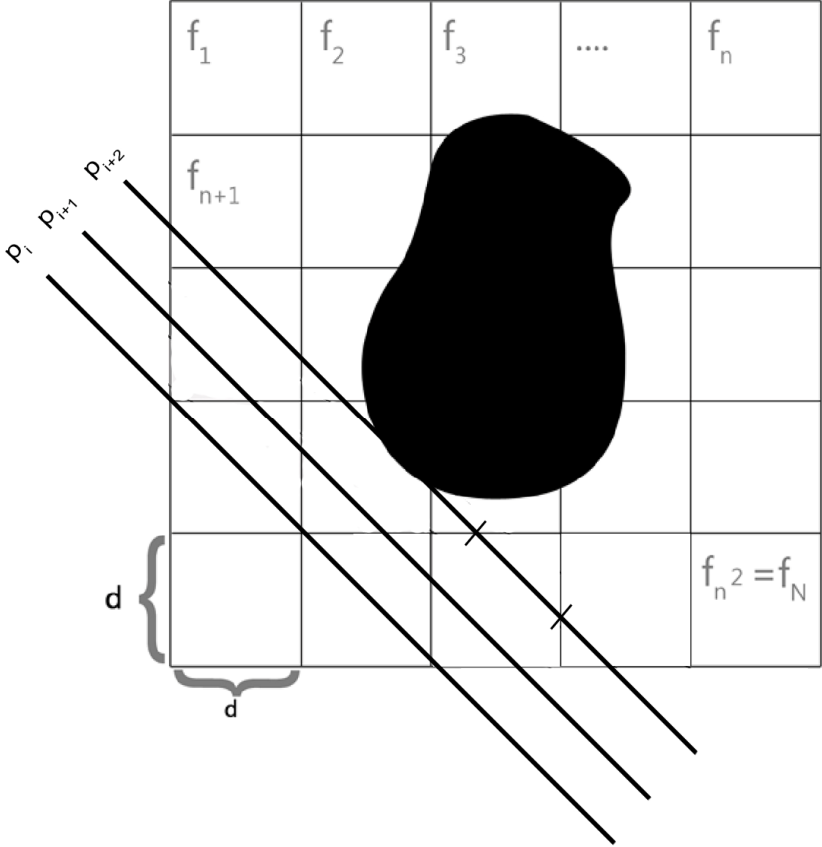


Figure 1.6: The square grid used in algebraic methods

Conventional matrix inversion methods mentioned above, would be useful to solve Equation (3) if M and N were small. Practical image grid size and required number of rays makes w_{ij} a large matrix inconvenient to be solved directly with matrix inversion or least squares method because of complex computation. Iterative methods are introduced for large values of N and M. Expanded form of the Equation(3) can be written as,

$$\begin{aligned}
w_{11}f_1 + w_{12}f_2 + w_{13}f_3 + \dots + w_{1N}f_N &= p_1 \\
w_{21}f_1 + w_{22}f_2 + w_{23}f_3 + \dots + w_{2N}f_N &= p_2 \\
\vdots & \\
w_{M1}f_1 + w_{M2}f_2 + w_{M3}f_3 + \dots + w_{MN}f_N &= p_M
\end{aligned} \tag{4}$$

If there is a unique solution to the Equation (4) then the intersections of the planes to be defined by these equations are a single point which gives the solution itself. This is known as the Kaczmarz method which forms the basis of ART. The implementation procedure starts with an initial guess, $\vec{f}^{(0)}$, at the solution and $\vec{f}^{(0)}$ is projected on the first plane in Equation (4) giving $\vec{f}^{(1)}$. Then $\vec{f}^{(1)}$ is projected on the second plane giving $\vec{f}^{(2)}$, thus the initial guess is updated so on. This procedure can be formulated as projection of $\vec{f}^{(i-1)}$ on i th plane yields $\vec{f}^{(i)}$;

$$f_j^{(i)} = f_j^{(i-1)} + \frac{(p_i - \sum_{k=1}^N f_k^{(i-1)} \cdot w_{ik})}{\sum_{k=1}^N w_{ik}^2} w_{ij} \quad \begin{matrix} j = 1, 2, \dots, N \\ i = 1, 2, \dots, M \end{matrix} \tag{5}$$

Equation (5) states that the previous intensity values of the estimated image, $f_j^{(i-1)}$, are updated by adding an error parameter $\Delta f_j^{(i)}$ which is the difference between measured ray-sum, p_i , and the computed ray-sum, $\sum_{k=1}^N f_k^{(i-1)} \cdot w_{ik}$, normalized by $\sum_{k=1}^N w_{ik}^2$. This process is repeated until all the projections are considered and all the pixel values converge to a solution [29, 30].

Different approximations can be proposed to define weighting parameters. The inconsistencies of these approximations can cause computational noise. One solution to suffer with the noise is multiplying the error with a relaxation parameter less than one, thus the intensity values of the pixels are updated by $\alpha \cdot \Delta f_j^{(i)}$. Relaxation parameter can be a constant or may decrease depending on the increase in the number of iterations.

Better image quality can be achieved if the update step is not applied ray by ray but after the error parameter is calculated for each ray. This method is called simultaneous iterative reconstruction technique (SIRT) which has a slower convergence than basic ART.

Superior results are obtained if the average of the error parameters generated by each ray after one iteration are applied to a pixel. This method is called simultaneous algebraic reconstruction technique (SART) and is driven as follows: for one iteration, normalized error of the first ray is calculated and stored in a correction array. The normalized error of the second ray is added to the correction array and after this procedure is carried out for all rays, the correction array is added to the image array. This method has the rapid convergence of ART and performs well in noise reduction like in SIRT. The reconstruction obtained with this method is shown in Equation (6) ;

$$f_j^{(i)} = f_j^{(i-1)} + \frac{\sum_i \left[\frac{(p_i - \sum_{k=1}^N f_k^{(i-1)} \cdot w_{ik})}{\sum_{k=1}^N w_{ik}^2} w_{ij} \right]}{\sum_i w_{ik}} \quad (6)$$

1.6 Hypothesis

In breast tomography the main constraint is the maximum radiation dose that can be given to the breast tissue which leads to a challenge in obtaining an accurate reconstruction in a limited angle of view. Tomosynthesis is a way to overcome this limitation. Algebraic reconstruction techniques are frequently used in tomosynthesis because it is easy to implement and incorporate prior knowledge in. The original purpose of this thesis is to develop an efficient ray tracing algorithm for image reconstruction from parallel beam projections of the 2D and to compare it with the known Siddon's algorithm with respect to the ray-sum theory of ART: Siddon's algorithm [31] which is a time efficient evolution of the radiological path and Gaussian algorithm is developed which enables to squeeze the image in direction of exposure and depicted as an alternative for Siddon. Each implementation is inserted in the algorithm of SART that is directly used to reconstruct images from projections acquired using analytical phantoms and the coding is performed in Matlab.

2. BACKGROUND

2.1 Ray Tracing Algorithms

The idea of ray tracing algorithms is to determine the indices of the voxels which are intersected by a given ray path that goes through the image array. This information is necessary to define exact weighting parameters for reconstruction of images. Several difficulties are associated with approximation of weighting parameters especially when enormous number of voxels and rays are in consideration. It seems very simple in geometric basis however it requires a significant computing time scales with the total number of voxels.

In 1985, Siddon proposed a fast and accurate algorithm to determine the exact radiological path. The computing time depends not on the number of voxels but number of the planes of the 3D image array. Therefore the algorithm is efficient and particularly straightforward to implement in computer code. It is preferred in many studies in different fields of medical imaging [31,32].

Another geometric approach in ray tracing is Gaussian model that will be considered here. In this method weighting parameters are accepted to be Gaussian parameters computed by the distance of the ray line to the center points of the pixels in 2D projection images. This method gives opportunity to squeeze the image in exposure direction with changing the parameter which controls the width in the Gaussian function.

2.1.1 Siddon's Algorithm

If Equation (3) is to be redefined, weighting parameter, w_{ij} , will be replaced by the length parameter, $l(i, j, k)$, which is a part of a certain ray-line intersected by a voxel. Therefore the ray-sum, in other words the radiological path, is defined by;

$$d = \sum_i \sum_j \sum_k l(i, j, k) p(i, j, k) \quad (7)$$

where $p(i, j, k)$ is the voxel density (attenuation coefficient).

Evaluation of Equation (7) requires an algorithm that scales with the number of terms in the sums which is the number of voxels in 3D space. In this algorithm, the knack is that the voxels are thought to be intersection volumes of equidistant parallel planes. The intersection points of the ray with the planes are calculated smoothly with the knowledge of the intersection point of the ray with the first plane and generating other intersection points of that ray with other planes by recursion. The 2D version of the method is illustrated in Figure 2.1 where the pixels are considered as the intersection areas of equally spaced parallel planes.

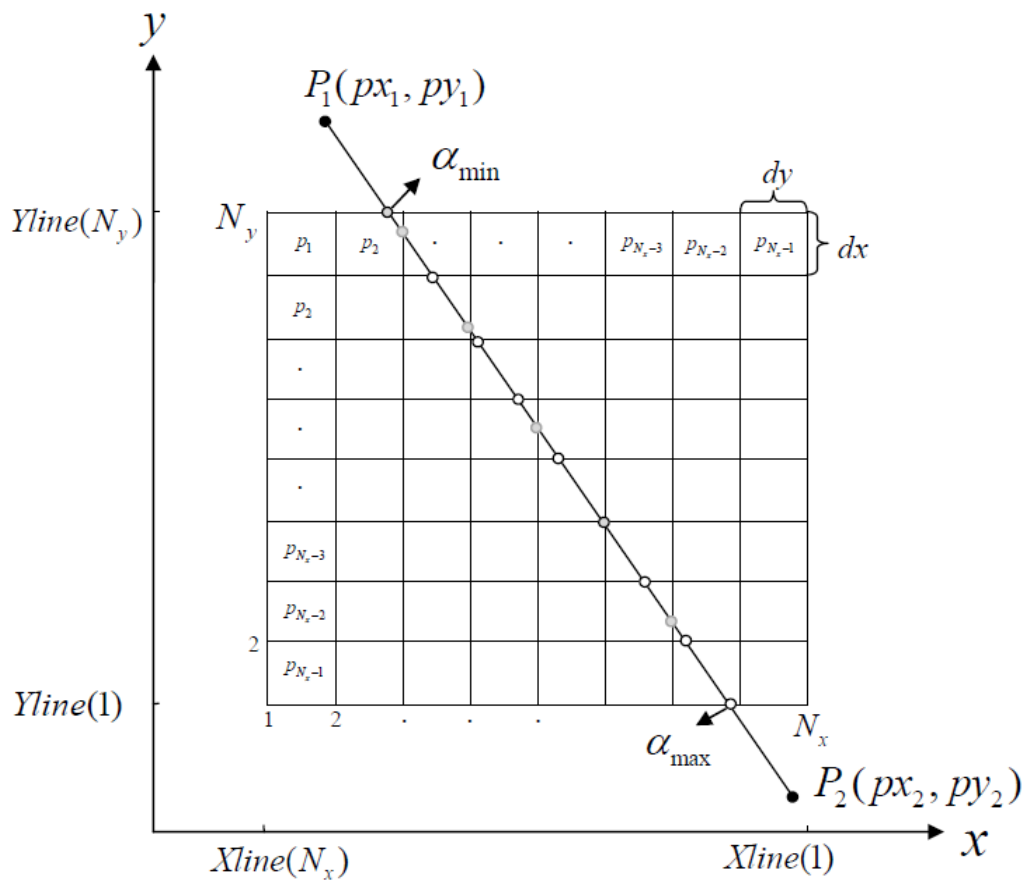


Figure 2.1: Geometric illustration of a ray on image grid

Figure 2.1 shows that intersection points are the union of two sets which includes the intersections of the ray with the horizontal lines (open circles) and one set with the vertical lines (closed circles). It is clearly seen that the intersections with the pixels are a subset of intersections with the lines.

In Siddon's algorithm, a ray from point 1 ($P1$) located on (x_1, y_1, z_1) to point 2 ($P2$) located on (x_2, y_2, z_2) is defined linearly by;

$$\begin{aligned} X(\alpha) &= X_1 + \alpha(X_2 - X_1), \\ Y(\alpha) &= Y_1 + \alpha(Y_2 - Y_1), \\ Z(\alpha) &= Z_1 + \alpha(Z_2 - Z_1), \end{aligned} \quad (8)$$

Where the parameter α is zero at point 1 and unity at point 2. Each intersection has an α parameter in the range of $(\alpha_{\min}, \alpha_{\max})$. If point 1 or point 2 lie on the image array the first and last intersection points will take the parameters α_{\min} and α_{\max} respectively.

For a $(Nx-1, Ny-1, Nz-1)$ voxels image array, the orthogonal sets of equidistant parallel planes are written as;

$$\begin{aligned} X_{plane}(i) &= X_{plane}(1) + (i-1)d_x & (i = 1, 2, \dots, Nx) \\ Y_{plane}(j) &= Y_{plane}(1) + (j-1)d_y & (j = 1, 2, \dots, Ny) \\ Z_{plane}(k) &= Z_{plane}(1) + (k-1)d_z & (k = 1, 2, \dots, Nz) \end{aligned} \quad (9)$$

where d_x , d_y and d_z are the distances between planes which are the size of the voxel. The maximum and minimum values for the α parameter are acquired with intersecting the ray with the sides of the image array. The parametric values of the sides are calculated from Equations (8) and (9) as follows;

If $(X_2 - X_1) \neq 0$,

$$\begin{aligned} \alpha_x(1) &= [X_{plane}(1) - X_1] / (X_2 - X_1), \\ \alpha_x(N_x) &= [X_{plane}(N_x) - X_1] / (X_2 - X_1), \end{aligned} \quad (10)$$

Expressions are similar for y and z directions. Depending on the location of the point 1 and 2, values for $(\alpha_{\min}, \alpha_{\max})$ are computed by merging the sets as in Equation (11),

$$\begin{aligned}\alpha_{\min} &= \max\{0, \min[\alpha_x(N_x)], \min[\alpha_y(1), \alpha_y(N_y)], \min[\alpha_z(1), \alpha_z(N_z)]\} \\ \alpha_{\max} &= \min\{1, \max[\alpha_x(N_x)], \max[\alpha_y(1), \alpha_y(N_y)], \max[\alpha_z(1), \alpha_z(N_z)]\}\end{aligned}\quad (11)$$

If α_{\max} is less than or equal to α_{\min} then it is obvious that the ray does not intersect the image array. The range of indices $(i_{\min}, i_{\max}), (j_{\min}, j_{\max})$ and (k_{\min}, k_{\max}) corresponding to the intersected planes which have parametric values in the range $(\alpha_{\min}, \alpha_{\max})$ are achieved as follows;

If $(X_2 - X_1) \geq 0$,

$$\begin{aligned}i_{\min} &= N_x - [X_{line}(N_x) - \alpha_{\min}(X_2 - X_1) - X_1]d_x \\ i_{\max} &= 1 + [X_1 + \alpha_{\max}(X_2 - X_1) - X_{line}(1)]/d_x\end{aligned}$$

If $(X_2 - X_1) \leq 0$ (12)

$$\begin{aligned}i_{\min} &= N_x - [X_{line}(N_x) - \alpha_{\max}(X_2 - X_1) - X_1]d_x \\ i_{\max} &= 1 + [X_1 + \alpha_{\min}(X_2 - X_1) - X_{line}(1)]/d_x\end{aligned}$$

with similar equations hold for $j_{\max}, j_{\min}, k_{\min}$ and k_{\max} .

The sets of parametric values which represent the intersections of the ray with all the planes can be written including the indice data using the notation for $\{\alpha_x\}$ and with similar notations for $\{\alpha_y\}, \{\alpha_z\}$;

$$\{\alpha_x\} = \{\alpha_x(i_{\min}), \dots, \alpha_x(i_{\max})\}; (X_2 - X_1) > 0 \quad (13)$$

where

$$\begin{aligned}\alpha_x(i) &= [X_{line}(i) - X_1]/(X_2 - X_1) \\ &= \alpha_x(i-1) + [d_x/(X_2 - X_1)],\end{aligned}$$

The definite intersection points are found by merging the sets $\{\alpha_x\}$, $\{\alpha_y\}$ and $\{\alpha_z\}$ into one set considering the ending points of the ray can be inside the array, therefore the maximum and minimum values are also added to the merged set.

$$\begin{aligned}\{\alpha\} &= \{\alpha_{\min}, \text{merge}[\{\alpha_x\}, \{\alpha_y\}, \{\alpha_z\}, \alpha_{\max}]\}, \\ &= \{\alpha(0), \dots, \alpha(n)\}\end{aligned}\quad (14)$$

The parameter set consists of $n+1$ elements where n is given as ;

$$n = (i_{\max} - i_{\min} + 1) + (j_{\max} - j_{\min} + 1) + (k_{\max} - k_{\min} + 1) + 1 \quad (15)$$

The intersection length, which means the weighting factor, can be defined in terms of the difference between the two adjacent terms in the set of α parameters. For two intersections m and $m-1$, the intersection length of the voxel is defined as;

$$l(m) = d_{12}[\alpha(m) - \alpha(m-1)] , \quad (m = 1, \dots, n) \quad (16)$$

where d_{12} is the total length of the ray from point 1 to point 2.

$$d_{12} = [(X_2 - X_1)^2 + (Y_2 - Y_1)^2 + (Z_2 - Z_1)^2]^{1/2} \quad (17)$$

The mid point of the two adjacent intersections, m and $m-1$, define the voxel indices $[i(m), j(m), k(m)]$ as in the following equation;

$$\begin{aligned}i(m) &= 1 + [X_1 + \alpha_{\text{mid}}(X_2 - X_1) - X_{\text{plane}}(1)] / d_x, \\ j(m) &= 1 + [Y_1 + \alpha_{\text{mid}}(Y_2 - Y_1) - Y_{\text{plane}}(1)] / d_y, \\ k(m) &= 1 + [Z_1 + \alpha_{\text{mid}}(Z_2 - Z_1) - Z_{\text{plane}}(1)] / d_z,\end{aligned}\quad (18)$$

where α_{mid} is given by

$$\alpha_{mid} = [\alpha(m) + \alpha(m-1)] / 2 \quad (19)$$

The radiological path in Equation 6 can be finally written as;

$$\begin{aligned} d &= \sum_{m=1}^n l(m) p[i(m), j(m), k(m)] \\ &= d_{12} \sum_{m=1}^n [\alpha(m) - \alpha(m-1)] p[i(m), j(m), k(m)] \end{aligned} \quad (20)$$

where $p(i, j, k)$ defines the voxel intensity. The main advantage of this algorithm is its computation time that is scaled with the number of the planes ($3N$) instead of number of voxels (N^3) [31].

2.1.2 Gaussian Algorithm

A new ray tracing algorithm is developed to solve the problem of limited data. The squared pixels are thought to be Gaussian circles which enable squeezing in the direction of projection and also smoother projections can be obtained as in Figure 2.2. The algorithm proceeds as follows: The object is assumed to lie on a $M \times N$ grid same as in previous algorithm. The weighting parameter used to calculate Equation (3) is now defined as Gaussian Parameter (GP) which is determined as a result of a Gaussian function rather than the intersection length and formed as follows,

$$p_{ij} = Ae^{-\frac{(x-x_j)^2 + (y-y_j)^2}{2\sigma^2}} \quad \begin{aligned} i &= (1, 2, 3, \dots, M) \\ j &= (1, 2, 3, \dots, N) \end{aligned} \quad (21)$$

Where $A = \frac{1}{\sigma\sqrt{2\pi}}$, x_i and y_i are the coordinates of the center point of the pixel at (i,j) and σ is a user defined parameter which controls the standard deviation of the Gaussian curve. In words, Equation (21) means that the GP of a pixel with the indices i and j , p_{ij} , is originated from the idea that the square shaped pixels are thought as Gaussian circles with the same center points as in the squared grid. The distance between the center point of the pixel to the ray line is used to calculate the GP.

If the ray-sum calculation is thought to be in y-direction then the y-directional parameters can be ignored because they end with the result of 1. Then Equation (21) can be modified as;

$$p_{ij} = Ae^{-\frac{d_{cl}^2}{2\sigma^2}} \quad (22)$$

where d_{cl} means the orthogonal distance between the center of the pixel to the ray line. The procedure goes with the calculation of the ray-sums as follows,

$$l_k = \sum_{ij} Ae^{-\frac{d_{cl}^2}{2\sigma^2}} \quad (23)$$

where k defines the number of the ray.

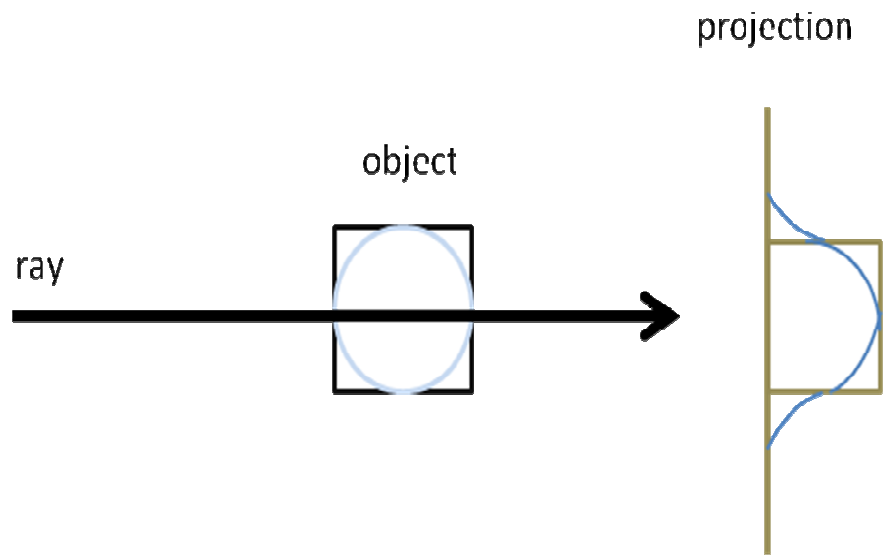


Figure 2.2: Smoothing with Gaussian form.

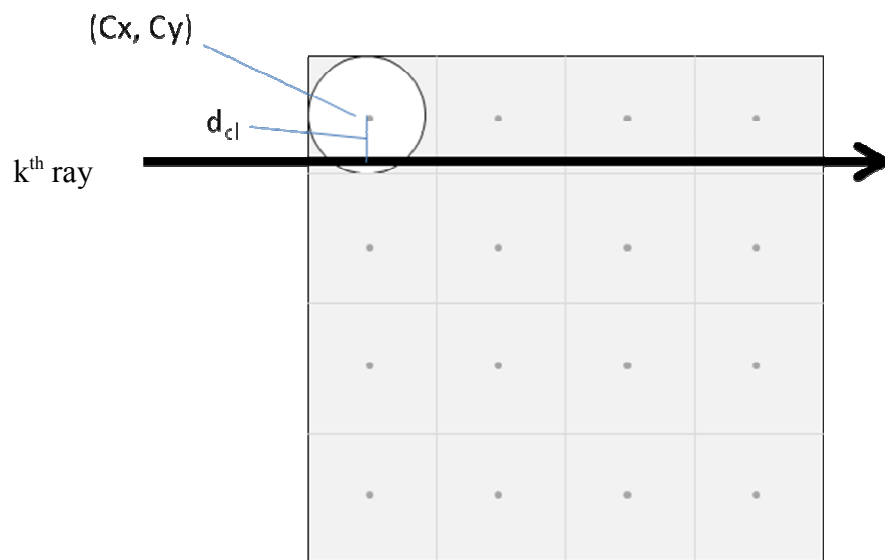


Figure 2.3: Geometric representation of the Gaussian algorithm.

3. METHODOLOGY

Inspired by tomosynthesis, in this thesis 2D image reconstruction with two ray tracing algorithms is studied in an iterative reconstruction framework. The first step of this study is the implementation part of the two ray-tracing algorithms. Firstly, Siddon's algorithm introduced above is slightly modified for 2D images by cancelling the parameters belong to z-direction. Intersection lengths obtained from Equation 16 are calculated for each ray at each angular position using a rotation matrix, R , to determine the new locations of $P1$ and $P2$.

$$R = \begin{pmatrix} \cos(\theta) & -\sin(\theta) \\ \sin(\theta) & \cos(\theta) \end{pmatrix}, \quad \theta = [0, \pi] \quad (24)$$

$$l_1 = \begin{pmatrix} x_{p1} \\ y_{p1} \end{pmatrix}$$

$$l_2 = \begin{pmatrix} x_{p2} \\ y_{p2} \end{pmatrix}$$

$$\begin{pmatrix} new_l_1 \\ new_l_2 \end{pmatrix} = R \times \begin{pmatrix} l_1 \\ l_2 \end{pmatrix} \quad (25)$$

In Equation (24) θ is the rotation angle, and in Equation (25) l_1 and l_2 are the locations of initial and final points of the ray respectively. The new locations after rotation are defined as new_l_1 and new_l_2 .

The intersection lengths of one ray with the grid pixels are exactly derived and located in a matrix of the grid size (length array). The projections are obtained by Equation (1) by replacing the weighing function with the length array.

The second algorithm, the Gaussian method, is implemented in the same manner by a squeezing process which is illustrated in Figure 3.1. The parallel X-ray beam is squeezed in the direction of the projection with a scale factor applied to the initial and final points of the rays such as;

$$\begin{pmatrix} y_{P1} \\ y_{P2} \end{pmatrix} = scale \times \begin{pmatrix} y_{P1} \\ y_{P2} \end{pmatrix} \quad (26)$$

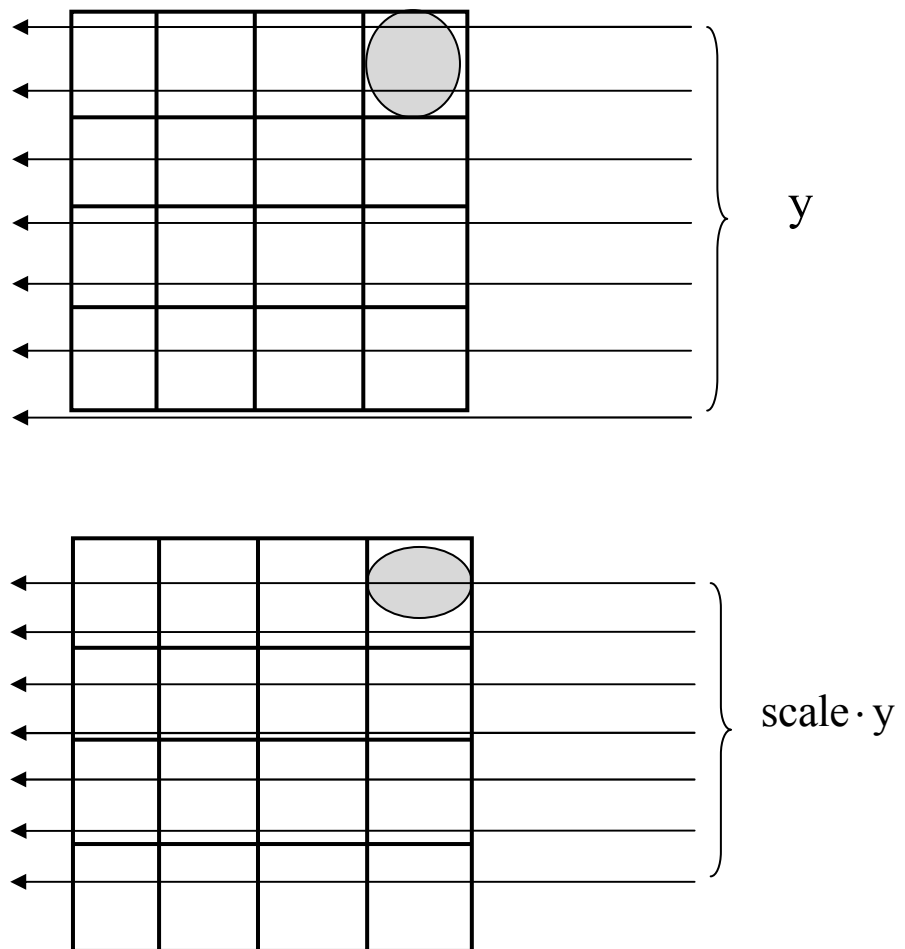


Figure 3.1: Squeezing process

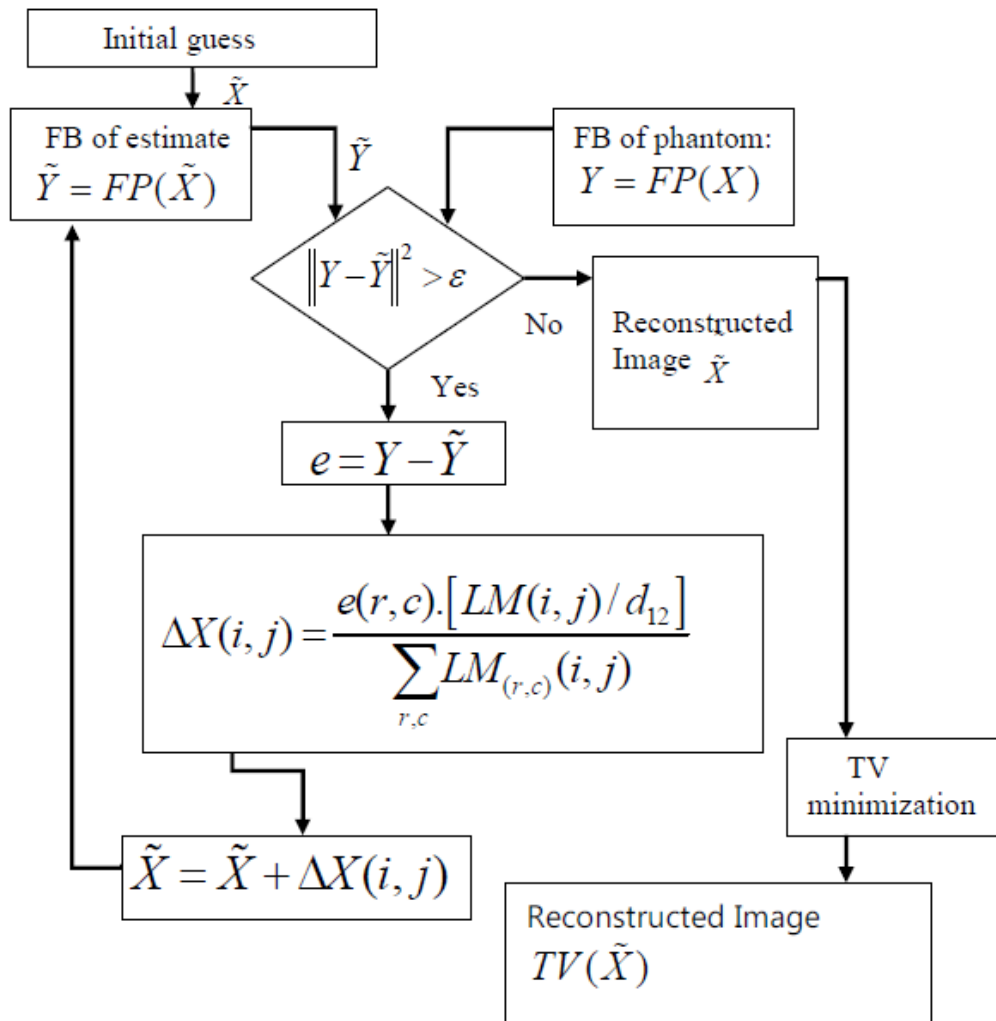


Figure 3.2: Flow chart of the SART algorithm

The distance between the pixel center and the ray line is also calculated including the same scale factor so that it is now no longer orthogonal. The scale factor is a user defined value between (0-1). A GP array is formed like the length array in Siddon's after the GPs are calculated for each ray and each position.

The third and most important step is to set up an algorithm for iterative reconstruction. SART is adapted to the results of these ray-tracing methods and the procedure takes the following steps also it is stated in a flow chart in Figure 3.2.

Step 1: Estimate an initial guess of the image \tilde{X} .

Step 2: Apply forward projection according to the ray-sum theory in Equation(3) using weighting parameters obtained from the ray-tracing methods.

Step 3: Update the image intensities with a correction array ΔX which is derived with a backward projection using SART.

$$\Delta X(i, j) = \frac{e(r, c)[LA(i, j) / d_r]}{\sum_{r, c} LA_{(r, c)}(i, j)} \quad (27)$$

where $e(r, c)$ is the error between the projection of the estimated image and the projection of the phantom for r 'th ray at c 'th angle. $LA(i, j) / d_r$ gives the proportion of the intersection length of a ray with the pixel, to the total length of the intersection of the ray with the image grid. $\sum_{r, c} LA_{(r, c)}(i, j)$ refers to the all intersection lengths of all rays that passes through one pixel.

Step 4: Impose the positivity control to the updated image such as ;

$$\tilde{X}(i, j) = \begin{cases} \tilde{X}(i, j), & \tilde{X}(i, j) \geq 0 \\ 0, & \tilde{X}(i, j) < 0 \end{cases} \quad (28)$$

Steps 2 to 4 is repeated until the convergence is achieved. The stopping criteria of the iterations is user defined and it is stated as a threshold value, ε , on the flow chart. The stopping criteria is based on the error between forward projections of the phantom and the estimated image and formulated as follows;

$$\frac{|SSE^{k+1} - SSE^k|}{SSE^k} > \varepsilon \quad (29)$$

where SSE refers to the sum of the squared error matrix.

In addition, a frame application as a substep to Step 4 can be added. Frame application means to set the definite *a priori* intensity values automatically to the estimated image at each step so that the reconstructed image appears to be less noisy. For instance, if a geometric boundary can be set to the object inside the grid as a field of interest, like in Figure 3.3, the pixels outside of this boundary gives zero intensity. Thus, there is no need to force the program to recompute these values. Frame application takes place in the flow chart as in Figure 3.4.

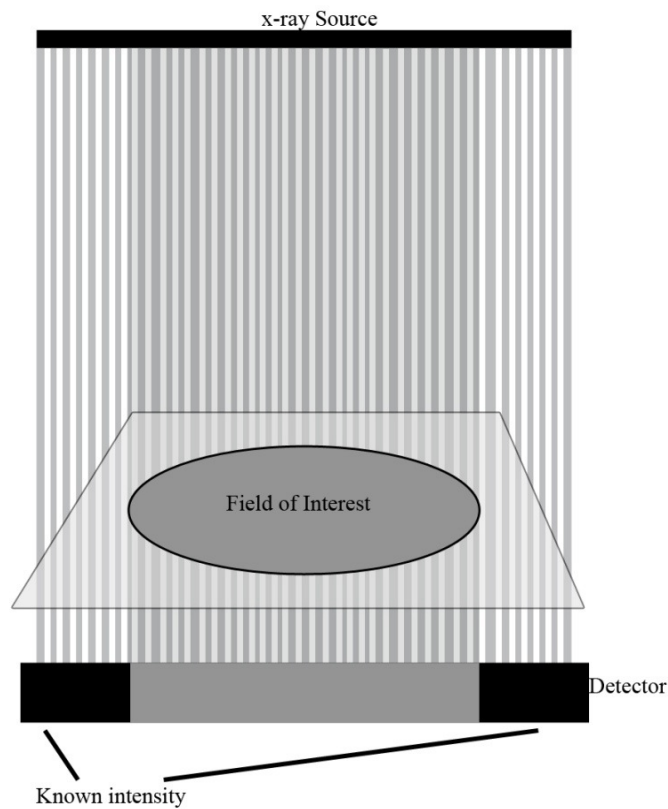


Figure 3.3: Frame application

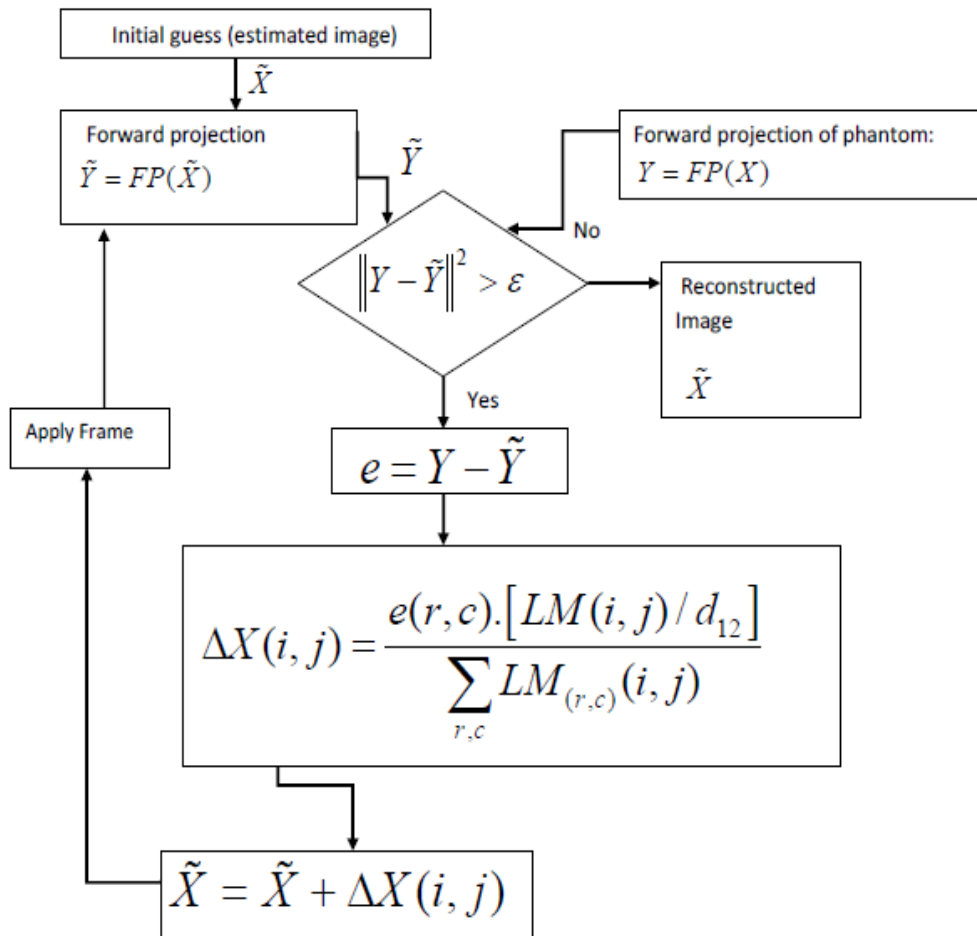


Figure 3.4 : Flow chart of the SART algorithm with frame application

3.1 Results

For numerical experiments a 2D phantom named *ploopgen* and *2D Shepp Logan* phantom of dimension 64×64 is chosen. The projections considering the noise-free case are obtained with Siddon's and Gaussian algorithm, programming in Matlab.

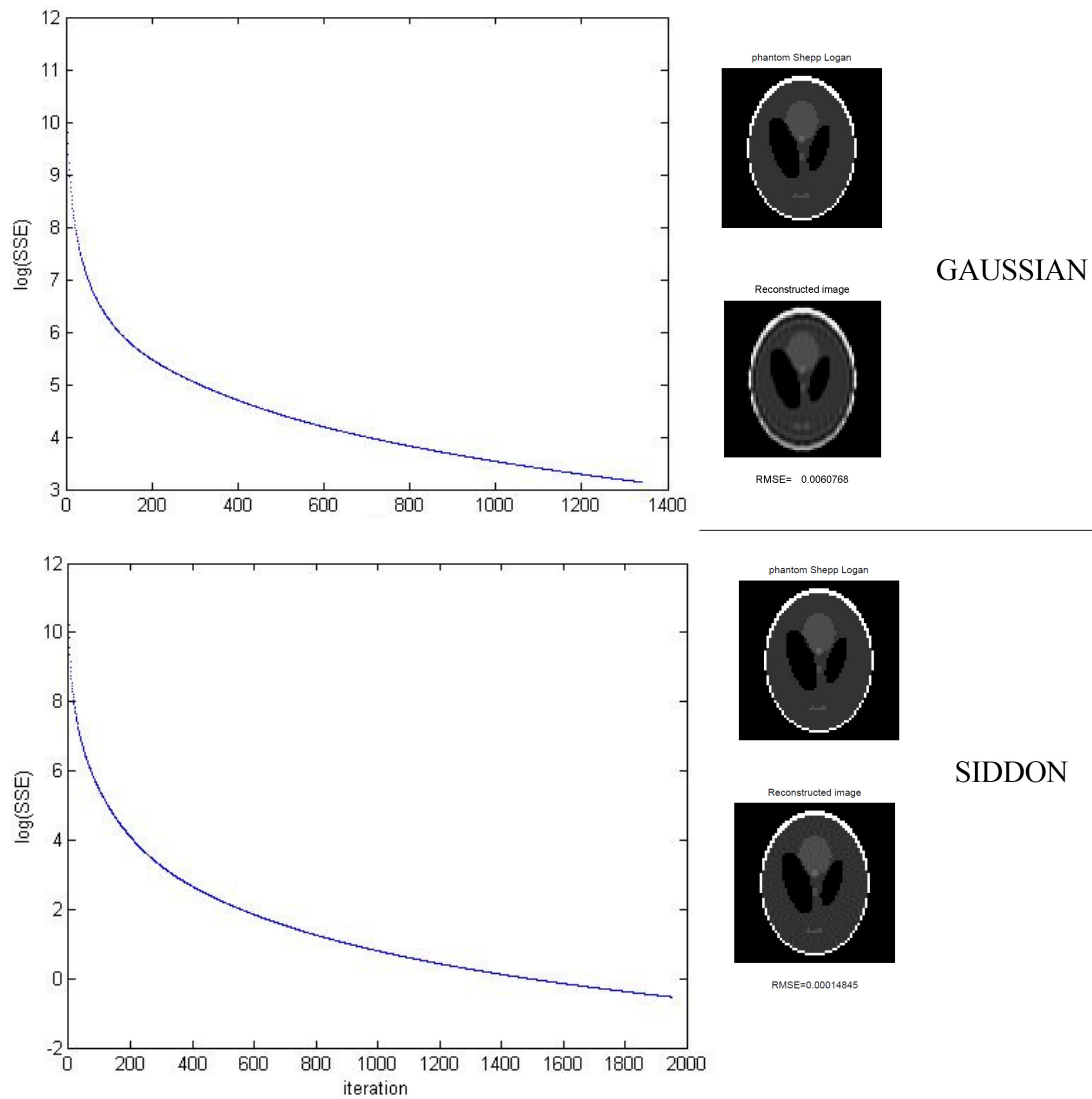


Figure 3.5: Convergence of the two ray tracing algorithm

Firstly in Figure 3.3, Shepp Logan phantom is projected without angle limitation with 50 projections -100 rays by two of the algorithms. It is shown that both of the algorithms are converging with SART with an SSE value of 0.001.

The difference of smoothing between Siddon's algorithm and newly developed Gaussian algorithm can be observed from the projections in Figure 3.6 and the following error chart. It is verified that both of the algorithms are working properly for full view of angle. Gaussian approach gives smoother results, however it is easily detectable by the frequency-based structure of the *ploopgen* phantom that the contrast in high frequencies are lower than the results of Siddon's algorithm.

The reconstruction success is determined by root mean square values of the error between the phantom and the reconstructed images as shown in Equation (30).

$$RMSE = \frac{\sum (\text{Phantom-Reconstructed Image})^2}{\text{image_size}} \quad (30)$$

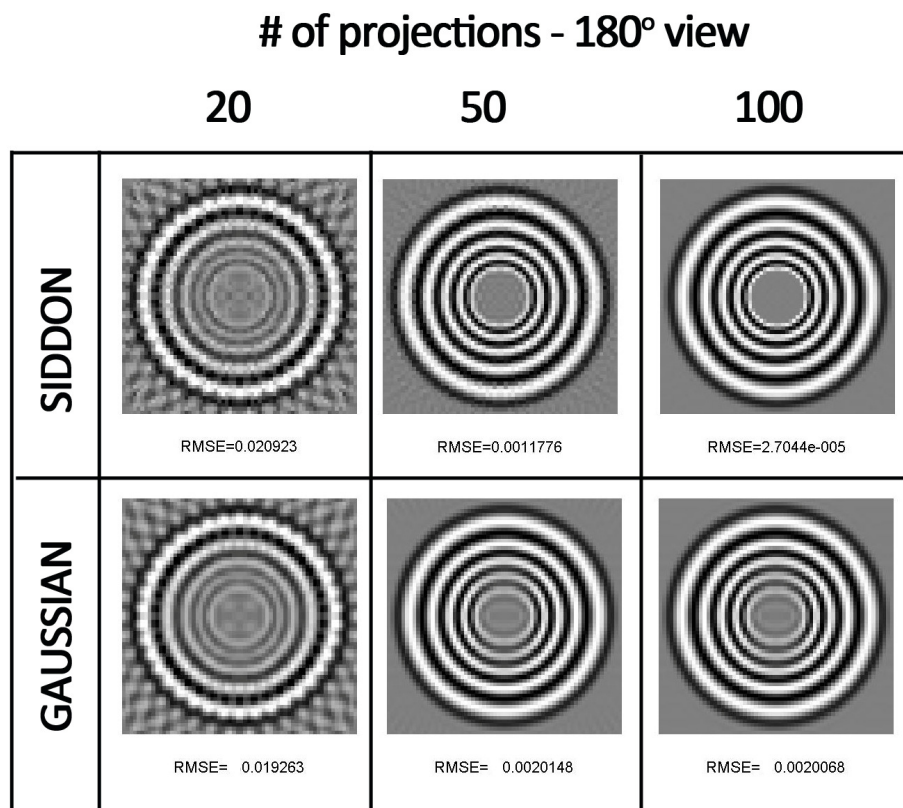


Figure 3.6: Comparison of the two ray tracing algorithms for full angle of view.

Number of Projections	RMSE	
	Siddon	Gaussian
20	0.020923	0.019263
50	0.0011776	0.0020148
100	2.7044*e-005	0.0020068

Table 3.1: RMSE Comparison of the two ray tracing algorithms for full angle of view.

Secondly, Figure 3.7 has the the results of Siddon’s Algorithm for four different number of projections and four different angle limitation. Figure 3.8 shows the results of Gaussian algorithm for the same conditions. The crux is reconstructing sufficient quality images from limited angle of view projections. It is clear to see that the image starts to be detectable at 90 degrees of limitation with 50 projections.

Third result is the frame application effects. When frame application is performed in 2D 64x64 Shepp-Logan phantom, the results of Gaussian algorithm with full view (π) show that the frame applied image is more close to the phantom.

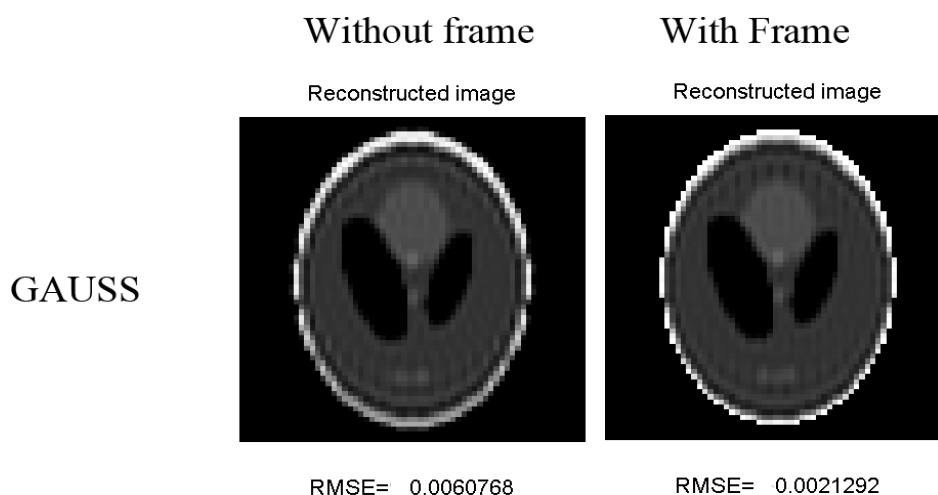


Figure 3.9: Frame application results for Gaussian algorithm


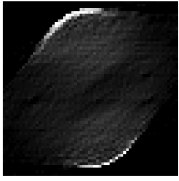
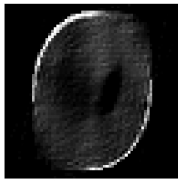

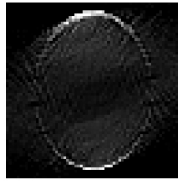



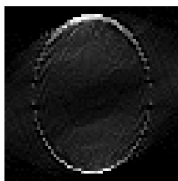
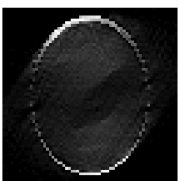


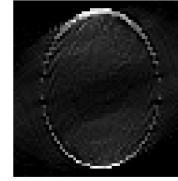
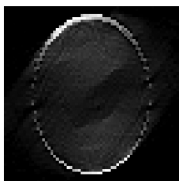


# of projections	angle range				
		30°	50°	90°	150°
10					
	RMSE=0.027282	RMSE=0.02426	RMSE=0.015692	RMSE=0.0068176	
20					
	RMSE=0.022657	RMSE=0.020921	RMSE=0.01189	RMSE=0.003667	
50					
	RMSE=0.019865	RMSE=0.015937	RMSE=0.0049706	RMSE=0.00031509	
100					
	RMSE=0.019491	RMSE=0.015624	RMSE=0.003471	RMSE=6.374e-005	

Figure 3.7: Results of the Siddon Algorithm



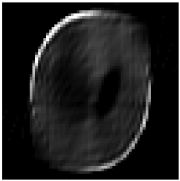
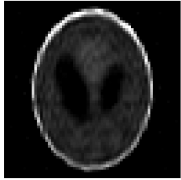


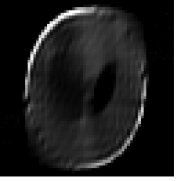

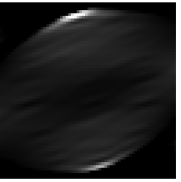
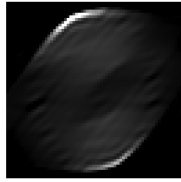
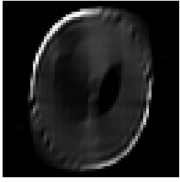

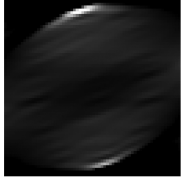
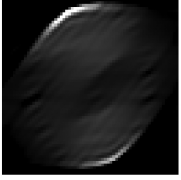
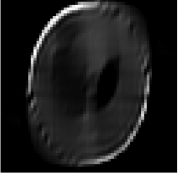
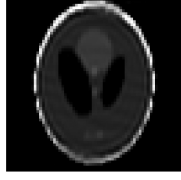
# of projections	angle range				
		30°	50°	90°	150°
10	Reconstructed image				
		RMSE= 0.030826	RMSE= 0.027585	RMSE= 0.016716	RMSE= 0.0082104
20	Reconstructed image				
		RMSE= 0.031956	RMSE= 0.027661	RMSE= 0.016579	RMSE= 0.0069143
50	Reconstructed image				
		RMSE= 0.032526	RMSE= 0.027803	RMSE= 0.016659	RMSE= 0.0064255
100	Reconstructed image				
		RMSE= 0.032712	RMSE= 0.027869	RMSE= 0.016772	RMSE= 0.0064325

Figure 3.8: Results of the Gaussian Algorithm

Degrees	30		50		90		100	
	Siddon	Gaussian	Siddon	Gaussian	Siddon	Gaussian	Siddon	Gaussian
Project.								
10	0.027282	0.030826	0.02426	0.027585	0.015692	0.016716	0.006817	0.0082104
20	0.022657	0.031956	0.020921	0.027661	0.011890	0.016579	0.003667	0.0069143
50	0.019865	0.0322526	0.015937	0.027803	0.0049706	0.016653	0.00031509	0.0064255
100	0.019491	0.032712	0.015624	0.027869	0.003471	0.016772	6.374*e-005	0.00664325

Table 3.2: Comparison of RMSE values for Siddon and Gaussian algorithms

4. CONCLUSION AND RECOMMENDATIONS

Breast cancer will keep its importance as women population is getting older. The only way to survive with this disease is early detection. The special structure of the breast tissue limits the researchers to get better images for detecting the tumor on early stage. Tomosynthesis is has become popular on breast cancer diagnosis since it enables to focus on the plane of interest and has advantages on image quality with less radiation dose. One type of the reconstruction methods that is frequently used in tomosynthesis is the algebraic reconstruction techniques which is used form in this thesis. The major purpose of this research was to develop a new ray tracing algorithm and compare it with the known Siddon's algorithm to be used in tomosynthesis. Both of the algorithms could be simulated and it is shown that they both converge for higher than 90 degrees range of projections. Gaussian algorithm is expected to give smoother results. Although our expectations come through, it is observed that this method loose contrast in higher frequencies compared with Siddon's algorithm.

Due to the iterative property of algebraic reconstruction technique and the computers capabilities which is used, the experiments took more than ten minutes each.

During this study digital mammography, tomosynthesis and image quality principles are analysed to explicate the results. The future work is to be on the reconstruction algorithm itself to improve limited view of angle projections by methods like compressed sensing.

REFERENCES

- [1] **Turkish Cancer Statistics Database.** Department of Cancer, Turkish Ministry of Health. 2009.
- [2] **The Ministry of Health of Turkey,** 2010. Health Statistics Yearbook, pp. 28.
- [3] **Yılmaz H.H., Yazıhan N., Tunca D., Sevinç A., Olcayto E. Ö., Özgül N., Tuncer N. M.,** 2010. Cancer Trends and Incidence and Mortality Patterns in Turkey. Japanese Journal of Clinical Oncology Advance Access, pp. 1-6.
- [4] **World health Organization,**2004. Health statistics and health information systems. Disease and injury regional estimates for 2004.
- [5] **Heddson B., Rönnow K., Olsson M., Miller D.,** 2007. Digital versus screen-film mammography: A retrospective comparison in a population-based screening program. European Journal of Radiology, pp. 420-425.
- [6] **Gold. R. H., Basset L.W. , Widoff B. E.,** 1990. Highlights of the history of mammography. Radiographics, 1990, pp. 1111-1130.
- [7] **Steen A. V., R. Tiggelen V.,** 2007. Short history of mammography: A belgian perspective. JBR–BTR, pp. 151-153.
- [8] **Fischer U., Hermann K. P. , Baum F.,**2006. Digital mammography: current state and future aspects. Eur Radiol, pp. 38-44.
- [9] **Hambly N. M., McNicholas M. M., Phelan N., Hargaden G. C., O’Doherty A., Flanagan F. L.,** 2009. Comparison of Digital Mammography and Screen- Film Mammography in Breast Cancer Screening: A Review in the Irish Breast Screening Program , *AJR* ; 193:1010–1018.
- [10] **Hendrick R. E., Pisano E. D., Averbukh A., Moran C., Berns E. A., Yaffe M. J., Herman B., Acharyya S. Gatsonis C.,** 2010. Comparison of Acquisition Parameters and Breast Dose in Digital Mammography and Screen-Film Mammography in the American College of Radiology Imaging Network Digital Mammographic Imaging Screening Trial . *AJR* ; 194:362–369.
- [11] **Mitsutomi I.,Hiroko T.S., Mari K., Yukihiisa S., Sonoe H.,** 2009. Comparison of reading time between screen-film mammography and soft-copied, full-field digital mammography. Breast Cancer 16:58–61.
- [12] **Pisano E. D., Gatsonis C., Hendrick E., Yaffe M., Baum J. K., Acharyya S., Conant E. F., Fajardo, L. L., Bassett L., D’Orsi C., Jong R. , Rebner M.,** 2005. Diagnostic Performance of Digital versus Film Mammography for Breast-Cancer Screening. The New England Journal of Medicine, October, pp. 1773-1783.

- [13] **Gennaro G., Maggio di C.** 2006. Dose comparison between screen/film and full-field digital mammography. *Eur Radiol* pp 16: 2559–2566.
- [14] **Pisano E. D., Yaffe M. J.,**2005. Digital Mammography. *Radiology*, Vol. 34 No 2, pp. 353-361.
- [15] **Schilling R. B., Cox J. D., Sharma S. R. D.,**1997. Advanced Digital Mammography. *Journal of Digital Imaging*, Vol 10, No 3, pp. 133-135.
- [16] **James J.J.,** 2004. The current status of digital mammography, *Clinical Radiology*, pp. 1–10.
- [17] **Yaffe, M.J.,** 1990. AAPM tutorial: physics of mammography-image recording process. *RadioGraphics*, 10, 341-363.
- [18] **Highnam R., Brady M.,** 1999. *Mammographic Image Analysis*. Kluwer Academic Publishers, pp. 31-34
- [19] **Elmore J. G., Armstrong K., Lehman C. D , Fletcher S. W. ,** 2005. Screening for Breast Cancer. *JAMA*, March 9, Vol 293, No. 10 pp. 1245
- [20] **Nees A.V.,** 2008. Digital Mammography: Are There Advantages in Screening for Breast Cancer?. *Acad Radiol*; pp. 401–407
- [21] **Aslund M.,** 2007. Digital Mammography with a Photon Counting Detector in a Scanned Multislit Geometry. Doctoral Thesis, Department of Physics Royal Institute of Technology Stockholm, Sweden.
- [22] **Lewin J. M., Niklason L.,** 2007. Advanced Applications of Digital Mammography: Tomosynthesis and Contrast-Enhanced Digital Mammography. *Seminars in Roentgenology*, pp. 243-244.
- [23] **Badea C. , Kolitsi Z., Pallikarakis N.,**2001. A 3D imaging system for in-theatre orthopedic applications based on Digital Tomosynthesis. *International Congress Series*, pp. 1209–1210.
- [24] **Dobbins J. T., Godfrey D. J.,** 2003. Digital Tomosynthesis: current state of art and clinical potential. *Physics in Medicine and Biology*, pp R65-R106.
- [25] **Li B., Avinasha G. B., Uppaluria R., Eberhard J. W., Claus B. E.H,** 2004. The impact of acquisition angular range on the z-resolution of radiographic tomosynthesis. *International Congress Series* pp 13– 18.
- [26] **Gennaro G., Toledano A., Maggio di C., Baldan E., Bezzon E., La Grassa M., Pescarini L., Polico I., Proietti A., Toffoli A., Muzzio P. C.,** 2010. Digital breast tomosynthesis versus digital mammography: a clinical performance study. *Eur Radiol* pp. 1545–1553.

- [27] Grant D. G., 1972. **Tomosynthesis: “A Three Dimensional Radiographic Imaging Technique**, IEEE Transactions on Biomedical Engineering, Vol. BME-19 No. 1, pp. 20-22.
- [28] **Taourel P., Merigeaud S., Aubert E., Millet I, Curros Doyon F., Lacroix J. Prat et J. Pujol X.**, 2009. Tomosynthésé: Luxe ou nécessité. J Radiol, pp. 1813.
- [29] **Wang B., Kenneth B., Denny Lee**, 2004. Algebraic Tomosynthesis Reconstruction. Medical Imaging, pp. 711-717
- [30] **Kak A. C., Slaney M.**, 1988. Principles of Computerized Tomographic Imaging. IEEE Press.
- [31] **Siddon R. L.**, 1985. Fast calculation of the exact radiological path for three dimensional CT array. Medical Physics, Mar/Apr, pp. 252-255.
- [32] **Han G., Liang Z., You J.**, 1999. A Fast Ray Tracing Technique for TCT and ECT Studies. Nuclear Science Symposium, 1999. Conference Record. IEEE .

CURRICULUM VITAE



Candidate's full name: Emine Can

Place and date of birth: Balıkesir/Turkey -09.05.1986

Permanent Address: Istanbul / Turkey

Universities and Colleges attended:

- **MSc.:** Istanbul Technical University, Biomedical Engineering MSE Programme , Istanbul,Turkey
- **MSc. Exchange :** Linköping University Department of Biomedical Engineering, Linköping, Sweden.
- **BA:** Hacettepe University Department of Electrical and Electronics Engineering, Ankara, Turkey

Publications:

- **Can, E., Yilmaz, A.** “Design of a neural modelling scheme for gait temporal features”, Signal Processing and Communications Applications Conference Book, 2009. SIU 2009. IEEE 17th, p 572-575.